Race Car Aerodynamics

Gregor Seljak

April 8, 2008

1 Introduction

First racing cars were primarily designed to achieve high top speeds and the main goal was to minimize the air drag. But at high speeds, cars developed lift forces, which affected their stability. In order to improve their stability and handling, engineers mounted inverted wings profiles[1] generating negative lift. First such cars were Opel's rocket powered RAK1 and RAK2 in 1928. However, in Formula, wings were not used for another 30 years. Racing in this era 1930's to 1960's occured on tracks where the maximum speed could be attained over significant distance, so development aimed on reducing drag and potencial of downforce had not been discovered until the late 1960's. But since then, Formula 1 has led the way in innovative methods of generating downforce within ever more restrictive regulations.

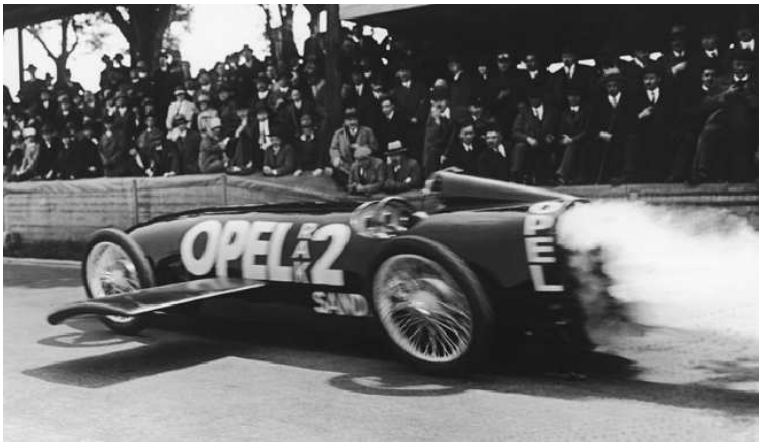

Figure 1: Opel's rocket powered RAK2, with large side wings

2 Airfoils

Airfoil can be definead as a shape of wing, as seen in cross-section. In order to describe an airfoil, we must define the following terms(Figure 2)

- The *mean camber line* is a line drawn midway between the upper and lower surfaces.
- The *leading and trailing edge* are the most forward an rearward of the mean camber line.

[1]Compared to an aircraft

- The *chord line* is a line connecing leading an trailing edge.
- The *chord length* is the distance from the leading to the trailing edge, measured along the chord line.
- The *camber* is the maximum distance between mean camber line and chord line.
- The *thickness* is the distance between the upper and lower surfaces.

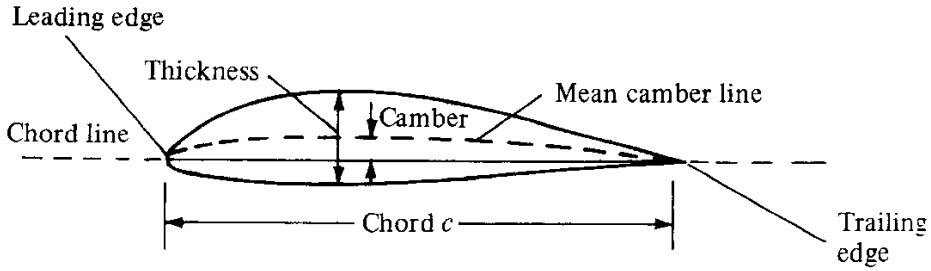

Figure 2: Airfoil nomenclature

The amount of lift L produced by the airfoil, can be expressed in term of *lift coefficient* C_L

$$L = \frac{1}{2}\rho_\infty V_\infty^2 S C_L \tag{1}$$

where V_∞ denotes the freestrem velocity, ρ_∞ fluid density and S the airfoil area.

2.1 Flow over an airfoil

Properties of an airfoil can be measured in a wind tunnel, where constant-chord wing spannes the entire test section, from one sidewall to the other. In this conditions, the flow sees a wing without wing tips. Such wing is called infinite wing and streches to infinity along the span. Because the airfoil section is identical along the wing, the properties of the airfoil and the infinite wing are identical. Therefore the flow over an airfoil can be described as a 2D incompressible inviscid flow over an infinite wing.

Lift per unit span L' generated by an arbitrary airfoil(or any other body) moving at speed V_∞ through the fliud with density ρ_∞ and circulation Γ is

given by Kutta-Joukowsky theorem

$$L' = \rho_\infty V_\infty \Gamma \,. \tag{2}$$

Circulation around an airfoil, can be calculated with the concept of a vortex sheet, which was first introduced by Prandtl an his colleagues. Consider an airfoil of arbitrary shape and thickness as shown in Figure 3. Circulation can be distributed over the whole airfoil area with surface density(vortex sheet strength) $d\Gamma/ds = \gamma(s)$, where $\gamma(s)$ must satisfy *Kutta condition*

$$\gamma(trailing\, edge) = 0 \tag{3}$$

Entire circulation is then given by

$$\Gamma = \int \gamma(s) ds \,, \tag{4}$$

where the integral is taken around the complete surface of the airfoil. However, there is no general solution for $\gamma(s)$ for an airfoil of arbitrary shape and it must be found numericaly, but analytical solutions can be found with some aproximations.

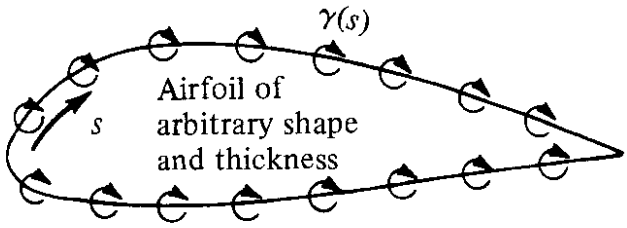

Figure 3: Simulation of an arbitrary airfoil by distributing a vortex sheet over the airfoil surface.

2.2 Thin airfoil theory

Here we discuss thin airfoil in freestream of velocity V_∞ under small angle of attack α. Camber and thickness are small in relation with chord length c. In such case, airfoil can be described with a single vortex sheet distributed over the camber line(Figure 4). Our goal is to calculate the variation of $\gamma(s)$, such that the chamber line becomes streamline and Kutta condition at trailing edge, $\gamma(c) = 0$, is satisfied.

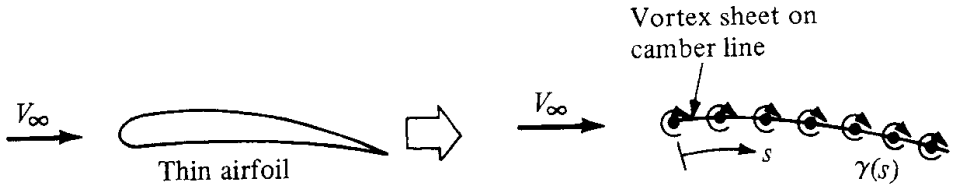

Figure 4: Thin airfoil approximation. Vortex sheet is distributed over the chamber line

The velocity at any point in the flow is the sum of the uniform freestream velocity and velocity induced by the vortex sheet . In order the camber line to be a streamline, the component of velocity normal to the camber line must be zero at any point along the camber line.

$$w'(s) + V_{\infty,n} = 0\,, \tag{5}$$

where $w'(s)$ is the component of velocity normal to the chamber line induced by the vortex sheet and $V_{\infty,n}$ the component of the freestrem velocity normal to the camber line. Considering small angle of atack and defining $\beta(x) = dz/dx$ as the slope of the chamber line, $V_{\infty,n}$ can be written as (Figure 5)

$$V_{\infty,n} = V_\infty\Big(\alpha - \frac{dz}{dx}\Big) \tag{6}$$

Because airfoil is very thin, we can make the approximation

$$w'(s) \approx w(x)\,, \tag{7}$$

where $w(x)$ denotes the component of velocity normal to the chord line and can be, using the Biot-Savart law, expressed as

$$w(x) = -\int_0^c \frac{\gamma(\xi)d\xi}{2\pi(x-\xi)} \tag{8}$$

Substituting equations (6), (7) and (8) into (5) and considering Kutta condition, we obtain

$$\begin{aligned} \frac{1}{2\pi}\int_0^c \frac{\gamma(\xi)d\xi}{x-\xi} &= V_\infty\Big(\alpha - \frac{dz}{dx}\Big) \\ \gamma(c) &= 0 \end{aligned} \tag{9}$$

fundamental equations of thin airfoil theory.

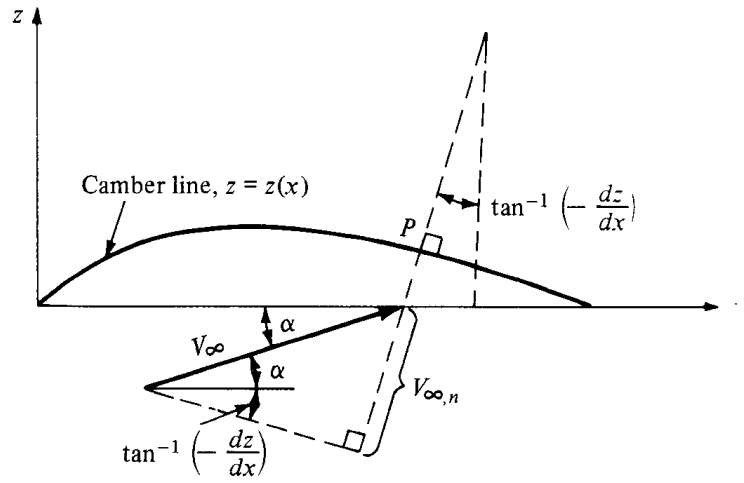

Figure 5: Determination of the component of freestrem velocity normal to the chamber line

In order to satisfy this conditions , we first transform our variables x and ξ into

$$\xi = \frac{c}{2}(1 - \cos\theta) \qquad x = \frac{c}{2}(1 - \cos\theta_0) \tag{10}$$

and equation (9) becomes

$$\frac{1}{2\pi}\int_0^\pi \frac{\gamma(\theta)\sin\theta d\theta}{\cos\theta - \cos\theta_0} = V_\infty\Big(\alpha - \frac{dz}{dx}\Big) \tag{11}$$

with a solution that satisfies Kutta condition $\gamma(\pi) = 0$

$$\gamma(\theta) = 2V_\infty\Big(A_0\frac{1+\cos\theta}{\sin\theta} + \sum_{n=1}^{\infty} A_n \sin(n\theta)\Big) \tag{12}$$

In order to find coefficients A_0 and A_n, we substitute equation (12) into equation (11) and use the following trigonometric relations

$$\int_0^\pi \frac{\sin(n\theta)\sin\theta d\theta}{\cos\theta - \cos\theta_0} = -\pi\cos(n\theta_0) \tag{13}$$

$$\int_0^\pi \frac{\cos(n\theta)d\theta}{\cos\theta - \cos\theta_0} = \frac{\pi\sin(n\theta_0)}{\sin\theta_0} \tag{14}$$

and finnaly obtain

$$\frac{dz}{dx} = (\alpha - A_0) + \sum_{n=1}^{\infty} A_n\cos(n\theta_0) \tag{15}$$

This equation is in form of a Fourier cosine series expansion for the function dz/dx. Comparing it to the general form for the Fourier cosine expansion we obtain

$$A_0 = \alpha - \frac{1}{\pi}\int_0^\pi \frac{dz}{dx} d\theta_0 \tag{16}$$

$$A_n = \frac{2}{\pi}\int_0^\pi \frac{dz}{dx}\cos(n\theta_0) d\theta_0 \tag{17}$$

The total circulation due to entire vortex sheet from leading to the trailing edge is

$$\Gamma = \int_0^c \gamma(\xi) d\xi = \frac{c}{2}\int_0^c \gamma(\theta)\sin\theta\, d\theta \tag{18}$$

Substituting equation (12) for $\gamma(\theta)$ into equation (18) and carrying out the integration, we obtain

$$\Gamma = cV_\infty\Big(\pi A_0 + \frac{\pi}{2}A_1\Big) \tag{19}$$

hence the *lift per unit span*, given by Kutta-Joukowski is

$$L' = \rho_\infty V_\infty \Gamma = c\rho_\infty V_\infty^2\Big(\pi A_0 + \frac{\pi}{2}A_1\Big) \tag{20}$$

This equation leads to to the *lift coefficient* in form

$$c_l = \pi(2A_0 + A_1) = 2\pi\Big[\alpha + \frac{1}{\pi}\int_0^\pi \frac{dz}{dx}(\cos(n\theta_0) - 1) d\theta_0\Big] \tag{21}$$

and *lift slope*

$$l_S \equiv \frac{dc_L}{d\alpha} = 2\pi \tag{22}$$

Last two results are important. We can see, that lift coefficient is function of the shape of the profile dz/dx and angle of attack α, and that even symmetrical wing produces lift, when set under an angle of attack. Lift slope is constant, independently of the shape of the profile, while the *zero lift angle*

$$\alpha_{L=0} = -\frac{1}{\pi}\int_0^\pi \frac{dz}{dx}(\cos(n\theta_0) - 1) d\theta_0 \tag{23}$$

depends on the shape. The more highly chambered the airfoil, the larger is $\alpha_{L=0}$

2.3 Viscid flow

By now, we have studied the inviscid incompressible flow. But in real case, flow is viscous. It is time to compare our theoretical results with real one. In Figure 6, we can see variation of lift coefficient with the angle of attack.

At low angles of attack c_l varies linearly with α, as predicted by the theory. However, at certain angle of attack, c_l reaches it's maximum value $c_{l,max}$ and starts to decrease. This is due to viscous effect of the fluid (air). First, the flow moves smoothly over the airfoil and is attached over most of the surface, but at certain value of α seperates from the top surface, creating a wake of turbulent flow behind the airfoil, which results in drop in lift and increase in drag.

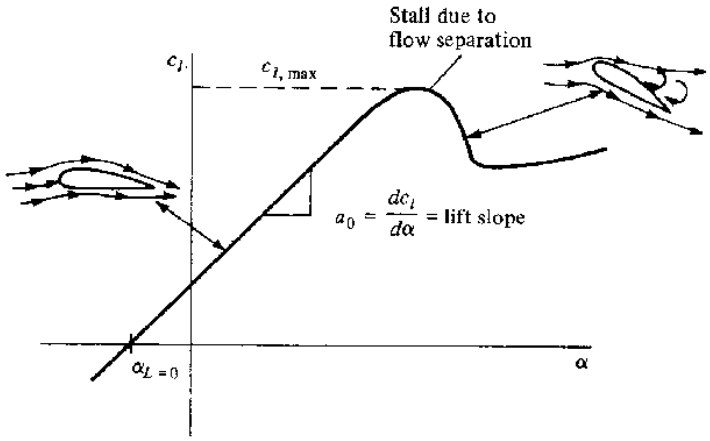

Figure 6: Variation of lift coefficient with the angle of atack.

To increase lift of the airfoil, we must increase $c_{l,max}$. As we have seen, the $c_{l,max}$ of the airfoil primarily depends on it's shape. Airfoil's shape can be changed with use of multielement *flaps* at the trailing edge and *slats* at leading edge. They increase chamber of the airfoil and therefore its $c_{l,max}$. The streamline pattern for the flow over such airfoil can be seen in Figure 7.

3 Finite wings

Properies of airfoils are the same as the properties of a wing of infinite span. However, all real wing are of finite span and the flow over finite wing is 3 dimensional. Because of higher pressure on the bottom surface of the wing, the flow tends to leak around the wing tips. This flow establishes a circulary motion that trails downstream of the wing. A *trailing vortex* is created at each wing tip. These wing-tip vortices induce a small downward component of air velocity, called *downwash* . It produces a local relative wind which is

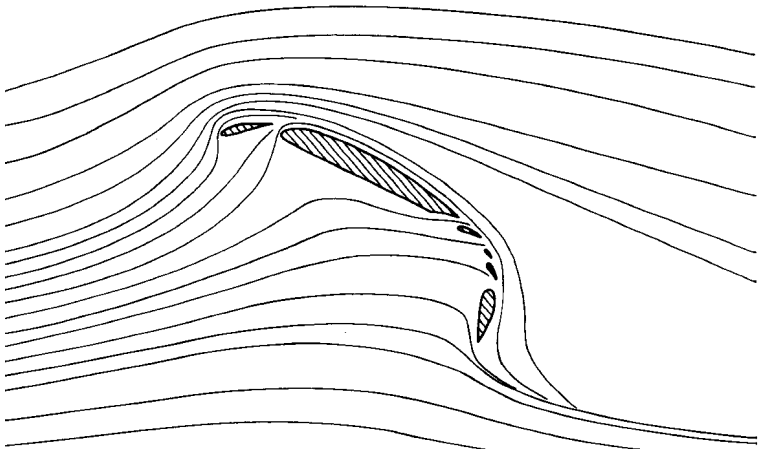

Figure 7: Flow over multielement airfoil.

directed downward in the vicinity of the wing, which *reduces* the angle of attack that each section of the wing effectively sees

$$\alpha_{eff} = \alpha - \alpha_i \tag{24}$$

and it creates a component of drag, defined as *induced drag*.

3.1 Prandtl's classical lifting-line theory

The idea of lifting line theory, is to use two dimensional results, and correct them for the influence of the trailing vortex wake and its downwash. Let's replace a finite wing of span b, with a *bound vortex*[2] extending from $y = -b/2$ to $y = b/2$. But due to the Helmholtz's theorem, a vortex filament can't end in a fluid. Therefore assume the vortex filament continues as two free vortices trailing downstream from the wing tips to infinity(Figure 8). This vortex is due to it's shape called *horseshoe vortex*. Downwash induced by such vortex, does not realistically simulate that of a finite wing, as it aproaches $-\infty$ at wing tips.

Instead of representing the wing by a single horseshoe vortex, Prandtl superimposed an infinite number of horseshoe vortices, each with an infinitesimally small strength $d\Gamma$, and with all the bound vortices coincident along a single line, called the *lifting line*. In this model, we have a continious distribution of circulation $\Gamma(y)$ along the lifting line with the value Γ_0 at the origin. The two trailing vortices in single horseshoe vortex model, have now

[2]A vortex bound to a fixed location in flow

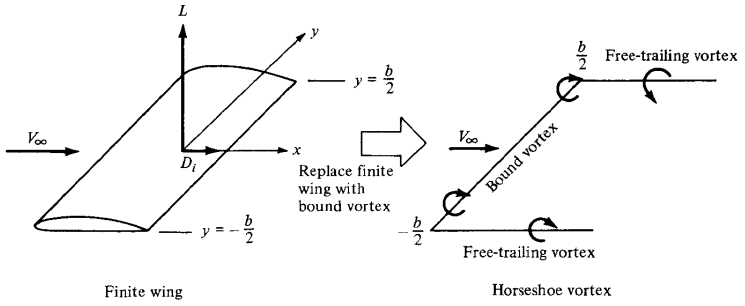

Figure 8: Replacement of the finite wing with single horseshoe vortex.

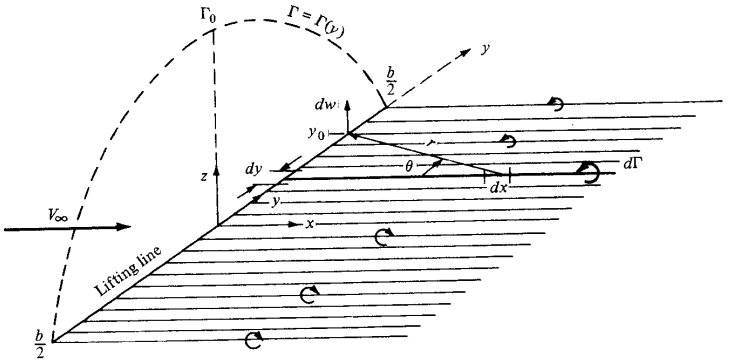

Figure 9: Superposition of an infinite number of horseshoe vortices along the lifting line.

became a continious vortex sheet trailing downstream of the lifting line,and the total downstream velocity w, induced at the coordinate y_0 by the entire trailing vortex sheet can be expressed as

$$w(y_0) = -\frac{1}{4\pi}\int_{-b/2}^{b/2} \frac{(d\Gamma/dy)dy}{y_0 - y} \tag{25}$$

The induced angle of attack at the arbitrary spanwise location y_0 is given by

$$\alpha_i(y_0) = \arctan\Big(\frac{-w(y_0)}{V_\infty}\Big) = \frac{-w(y_0)}{V_\infty}\,, \tag{26}$$

where we considered $V_\infty \gg w(y_0)$ and $\arctan(\alpha) \approx \alpha$ for small values of α. Now we can obtain an expression for the induced angle of attack in term of the circulation distribution along the wing

$$\alpha_i(y_0) = -\frac{1}{4\pi V_\infty}\int_{-b/2}^{b/2} \frac{(d\Gamma/dy)dy}{y_0 - y} \tag{27}$$

Combining results

$$c_l = \frac{2\Gamma(y_0)}{V_\infty} \tag{28}$$

and

$$c_l = 2\pi[\alpha_{eff}(y_0) - \alpha_{L=0}] \tag{29}$$

for coefficient of lift per unit span from thin airfoil theory, we obtain

$$\alpha_{eff} = \frac{\Gamma(y_0)}{\pi V_\infty c(y_0)} + \alpha_{L=0} \tag{30}$$

Substituting equations (27) and (30) into (24), we finally obtain the fundamental equation of Prandtl's lifting line theory.

$$\alpha(y_0) = \frac{\Gamma(y_0)}{\pi V_\infty c(y_0)} + \alpha_{L=0}(y_0) + \frac{1}{4\pi V_\infty}\int_{-b/2}^{b/2} \frac{(d\Gamma/dy)dy}{y_0 - y} \tag{31}$$

Just as in thin airfoil theory, this integral equation can be solved by assuming a Fourier series representation for the distribution of vorticity

$$\Gamma(\Theta) = 2bV_\infty \sum_{n=1}^{N} A_n \sin n\Theta \tag{32}$$

where we considered transormation $y = (-b/2)\cos\Theta$, with $0 \leq \Theta \leq \pi$ and coefficients A_n must satisfy Equation (31). With such vorticity distribution, Equation (31) becomes

$$\alpha(\Theta_0) = \frac{2b}{\pi c(\Theta_0)} \sum_{n=1}^{N} A_n \sin n\Theta_0 + \alpha_{L=0}(\Theta_0) + \sum_{n=1}^{N} nA_n \frac{\sin n\Theta_0}{\sin\Theta_0} \tag{33}$$

The total lift distribution is obtained by integrating equation for lift distribution over the span

$$L = \int_{-b/2}^{b/2} \rho_\infty V_\infty \Gamma(y)dy \tag{34}$$

Coefficients of lift and induced drag[3], can be calculated via equations

$$C_L = \frac{L}{q_\infty S} = \frac{2}{V_\infty S}\int_{-b/2}^{b/2} \Gamma(y)dy \tag{35}$$

and

$$C_D = \frac{D}{q_\infty S} = \frac{2}{V_\infty S}\int_{-b/2}^{b/2} \alpha_i(y)\Gamma(y)dy \tag{36}$$

[3]Note the difference in nomenclature. For 2D bodies, coefficients have been denoted with lowercase letters. In 3D case, we use capital letters

respecteviliy. Considering expressions (32) and (33), they can be written as

$$C_L = A_1 \pi AR \tag{37}$$

and

$$C_{D,i} = \frac{C_L^2}{\pi AR}(1+\delta) \tag{38}$$

where AR is *aspect ratio* of finite fing, defined as $AR = b^2/S$, and $\delta = \sum_2^N (A_n/A - 1)^2$. Note that C_L depends only on the leading coefficient in Fourier series expansion and that $\delta \geq 0$. Therefore, the lowest induced drag will be produced by a wing where $\delta = 0$, that is, $n = 1$. Such circulation distribution is given by $\Gamma(\Theta) = 2bV_\infty A_1 \sin\Theta$ and is known as *elliptical circulation distribution*

4 Ground effect

The main differece between wing application in aviation and car racing is, that cars are in contact with the ground. Therefore, wing experiences some additional effects due to ground proximity. Remember the wing tip vortices we mentioned at the beginning of the previous section. They do nothing but harm, as they increase drag and decrease lift at given angle of attack. When flying near to the ground, the ground partially blocks(Figure 10) the trailing vortices and decreases the amount of downwash generated by the wing. This reduction in downwash increases the effective angle of attack of the wing so that it creates more lift and less drag than it would otherwise. This effect is greater, the closer to the ground the wing operates.

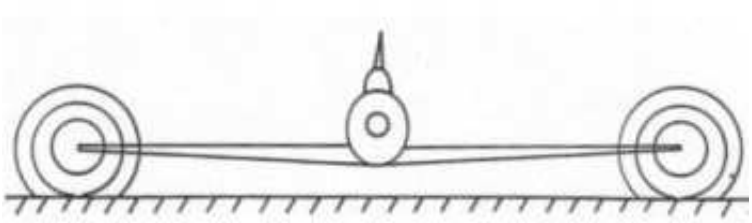

Figure 10: Effect of the ground proximity on creation of the trailing vortices.

Another way to create downforce is to create low pressure area underneath the car, so that the higher pressure above the car will apply a downward force. The area between car's underbody and the ground, can be thougth as an example of Venturi nozzle. The Venturi effect may be derived from

a combination of Bernoulli's principle and the equation of continuity. The fluid velocity increases through the constriction to satisfy the equation of continuity, while it's pressure decreases due to conservation of energy. The gain in kinetic energy is supplied by a drop in pressure. The main advantage of ground effect is, that it produces almost no drag.

5 Applications in car racing

Now summarize what we have learned so far. The coefficient of lift increases with increasing angle of attack. At some angle, flow seperates from the wing, which causes drop of lift coefficient. With use of multidimensional flaps, we increase chamber of the airfoil and thus maximum coefficent of lift.

In 3 dimensional case, vortices appear at wing tips. They reduce wing's efficiency and increase drag. The lowest drag can be achieved with elliptically shaped wing. Dimensions of the wing are also important. Wing with greater surface, produces more lift and wing with higher aspect ratio induces less air resistance.

In the next sections, we will see, how engineers used this principles at developing the main aerodynamical parts of racing cars.

5.1 Rear wing

First rear wing appeared in 1966, when Jim Hall equiped his Chaparral 2E with a rear wing. From then on, use of wings grew quickly. First wings were mounted high over the rear end of the car to operate in indisturbed flow. They were also mounted on pivots, so the driver was able to change the angle of attack during the ride. High mounted wings often broke off during the race and were therefore prohibited by FIA. In Formula 1, wings were first introduced in 1968 at the Belgium grand prix, when Ferrari used full inverted rear wings, and Brabham did likewise, just one day after the Ferrari's wings first appeared.

Modern rear wings produce approximately 30-35 % of the total downforce of the car. A typical configuration(Figure) consists of two sets of airfoils connected to each other by the wing endplates. The most downforce is provided by the upper airfoil. To achieve the greatest possible lift coefficient, it consists of multiple high aspect ratio elements, which prevent flow separation. Angle of attack depends on circuit configuration. On tracks with many turns, more downforce is needed, therefore the wing is set at higher angle of attack. Conversely, on tracks with long straights, wing has small angle attack, thus reducing air drag and allowing higher top speeds. Lower airfoil section ac-

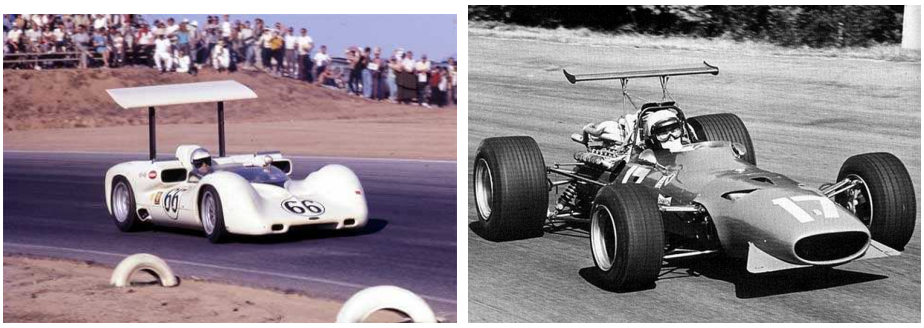

Figure 11: Chapparal 2E (left) and Ferrari 312 (right).

tually reduces the downforce produced by total rear wing, but it creates a low-pressure region just below the wing to help the diffuser[4] to create more downforce below the car. Ususally it consists of two elements.

Another important part of rear wing are endplates . They provide a convenient way of mounting wings, but also have aerodynamic function. They reduce the 3D effect of the wing by preventing air leakage around the wing tips and thus formation of trailing vortices. An additional goal of the rear endplates is to help reduce the influence of upflow from the rear wheels. The U-shaped cutout from the endplate further alleviates the development of trailing vortices.

5.2 Front wing

The front wing on the car produces about 1/3 of the car's downforce and it has experienced more modifications than rear wing. It is the first part of the car to meet the air mass, therefore, besides creating downforce, it's main task is to efficiently guide the air towards the body and rear of the car, as the turbulent flow impacts the efficiency of the rear wing.

Front wings appeared in Formula 1 just two weaks after the first rear wings, on Lotus 49B. First front wings were quite simple with single rectangular airfoil with flat vertical endplates to reduce wing tip vortices. First improvement appeared in 1971, with so-called Gurney flap. This is a flat trailing edge flap perpendicular to the chord and projects about 2% of the chord. It can improve the performance of a simple airfoil to nearly the same level as a complex design. The same year, the concept of elliptical wing was applied. March equiped it's 711 with elliptical front wing. Two years later Ferrari avoided wing-body interaction with wing mounted quite far ahead

[4]See section 5.3

Figure 12: Modern rear wing consists of upper(2) an lower(3) airfoil section mounted on endplates (1) with U-shaped cutout (4).

from the body. Multi element wings were introduced in 1984 by McLaren. The angle of attack of the second element was allowed to be modified so that the load applied on the front wing could be changed to balance the car according to the driver's wishes. In 1990 Tyrell raised the nose of it's 019 to increase the flow under the nose cone and improve flow conditions under the car. This concept avoids wing-body interaction and allows the front wing to operate in undisturbed flow. It also enlarges effective area of the wing. After Imola 1994, the FIA regulations do not allow any chassis parts under a minimum ground height. This clearance is different between the centre and the side of the car. Teams used this to curve front wing in the centre of the span and regain some of the lost ground effect. In 1998, regulations decreased the width of Formula 1 car, so the front wings overlapped the front wheels. This created unnecessary turbulence in front of the wheels and reducing aerodynamic efficiency of the wing. With reducing wing's span this could be avoided, but it would also decrease wing's aspect ratio. Insted this, teams use wing tips to direct the air around the wheels.

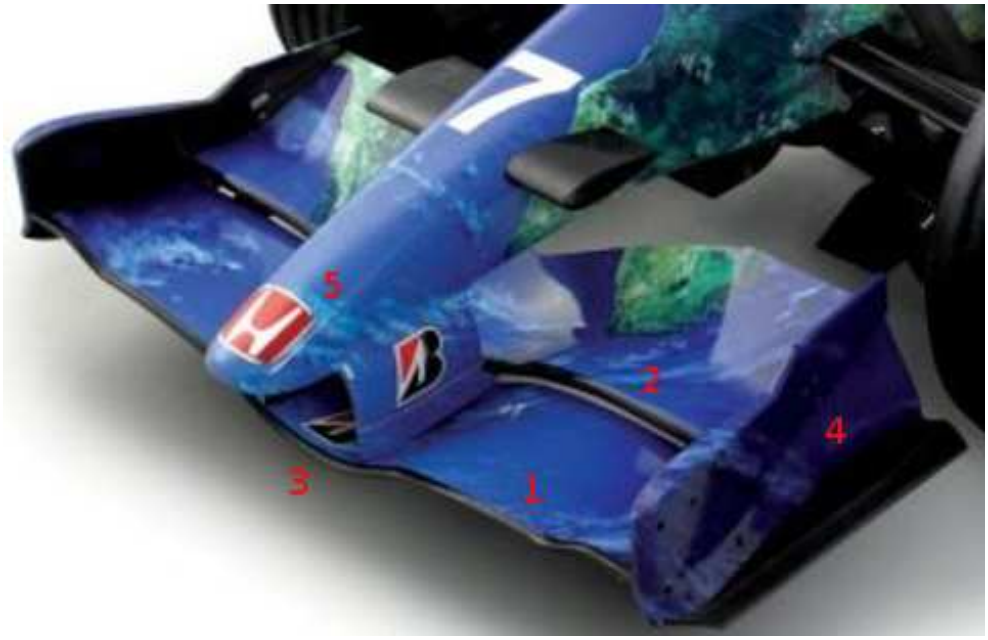

Figure 13: Configuration of modern front wing. Two element airfoil (1 & 2) is mounted under the nose of the car (5). Endplates (4) direct air around the wheels and curved area (4) under the nose increases wing's efficiency.

5.3 Ground effect

The second revolution in Formula 1 aerodynamics occurred about a decade after the first, with the introuction of the Lotus T78 in 1977. Lotus T78 and it's further development, Lotus T79, were first cars to use ground effect. The underbody took shape of inverted wing profile(Figure). The decreasing cross-sectional area accelerated the airflow and created low pressure underneath the car. The gap between the bottom of the sidepods and the ground was sealed with so-called sidepods. They helped to maintain 2D flow characteristics that provide increased downforce and reduced drag, compared to a typical 3D wing. Skirts enabled very high cornering speeds and were prohibited by the rules, due to safety reasons and from 1983 onwards, the tehnical regulations in Formula 1 require the underbody panel between the wheels to be completely level.

The flow wolume between the vehicle and the ground is strongly dependent on the car's attitude relative to the ground. This correlation is illusrtated in Figure. Very small ground clearence results in positive lift, since there is almost no airflow between the underbody and the ground. With in-

Figure 14: Some historical milestones in front wing develpment. Lotus 49B, March 711, Ferrari 312 T2 and Tyrrell 019.

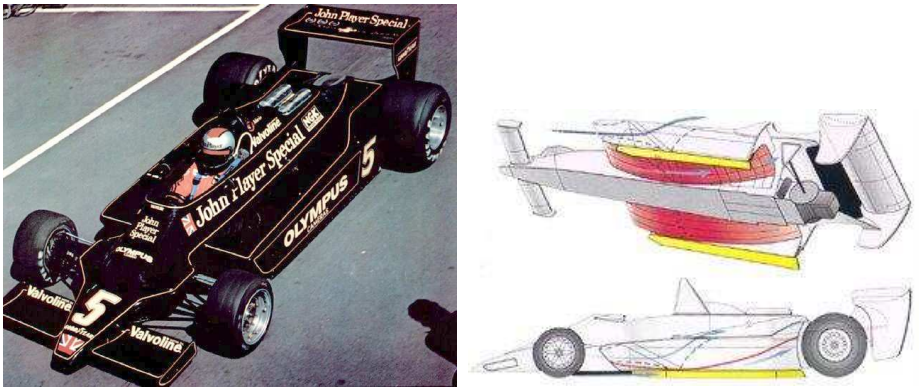

Figure 15: Lotus T79 and sketch of it's underbody

creasing ground clearence the airflow produces low pressures causing overall lift to be lowered to negative values and then to rise again as ground clearence continues to increase. This is due to the fact that the flow velocity under the car decreases as ground clearence increases. More downforce can be generated using a diffusor between the wheels at the rear of the car.The air enters the diffuser in a low-pressure, high-velocity state after accelerating under the

car. By gradually increasing the cross-sectional area of the diffuser, the air gradually slows down and returns to its original free-stream speed and pressure. The diffuser's aim is to decelerate the air without it separating from the tunnel walls, which would cause a stall, reducing the downforce and inducing a large drag force. By installing an inverted wing close to the diffuser exit [5] it is possible to create a low-pressure area, which essentially sucks the air from the diffuser. The diffuser and wing combination permits a higher air mass flow rate through the diffuser, thus resulting in higher downforce. Sharp edges on the vertical tunnel walls generate vortices from entrained air and help confine the air through the diffuser and reduce the chance it will separate.

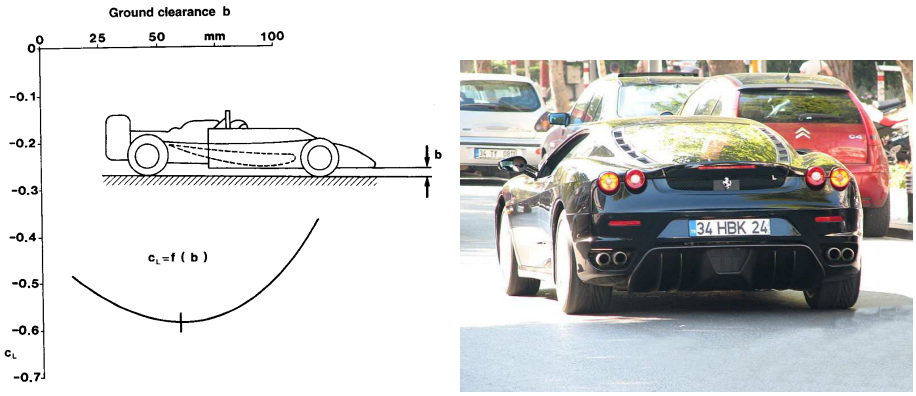

Figure 16: Correlation between lift coefficient and ground clearence(left) and diffuser on Ferrari F430(right)

Again Chaparral, showed completely new way to create downforce. The Chaparral 2J in 1969 used two rear fans to suck in air from under the car, thus creating low pressure under the car. Big advantage of this concept is, that downforce can be generated independently of the speed. Fans were also used in Formula 1. Brabham BT46 used a rear mounted fan driven off the gearbox. It won it's debut race in 1978, but was promptly banned by the governing body.

Barge boards were first seen in 1993 and their purpose is to smooth the airflow around the car and into the radiator intakes. They are most commonly mounted between the front wheels and the sidepods (See Figure) .Their main purpose is to direct relatively clean air into the sidepods.Clean air is from the low section of the front wing where airflow is fairly unaffected

[5]See rear wing section

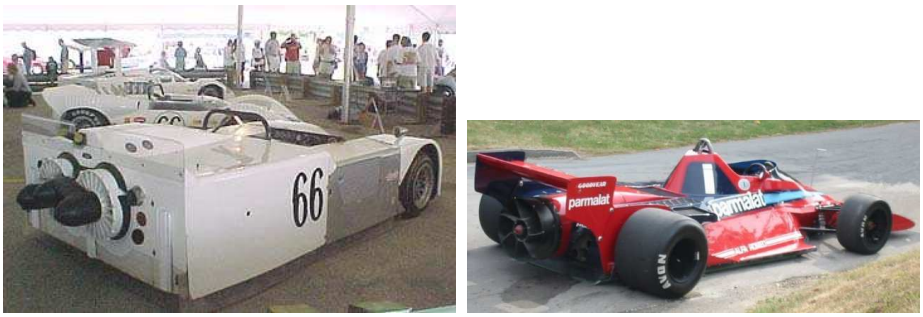

Figure 17: Two cars which used fans to create downforce. The Chaparral 2J "sucker car" (left) and Brabham BT46 "fan car"

by the wing and far away from tires, which may throw stones and debris in to the radiator. Bargeboards also produce vortices, to seal the area between the sidepots and the surface. They work as a substitude for skirts.

Figure 18: Bargeboards on McLaren MP4/8

6 Conclusion

References

[1] J. D. Anderson; *Fundamentals of Aerodynamics*

[2] Applied Aerodynamics: A Digital Textbook, http://www.desktopaero.com/appliedaero/preface/welcome.html

[3] W-H Hucho: *Aerodynamics of Road Vehicles*

[4] Peter Wright: *Formula 1 Technology*

[5] Milliken,Milliken: *Race Car Vehicle Dynamics*

[6] F. Mortel: *Cranfield Team F1: The Front Wing*